bioRxiv preprint doi: https://doi.org/10.1101/829234; this version posted November 4, 2019. The copyright holder for this preprint (which was not certified by peer review) is the author/funder. All rights reserved. No reuse allowed without permission.

Stability of cortical synapses across sleep and wake

Brian A. Cary[1], Gina G. Turrigiano[1,*]

1: Dept of Biology, Brandeis University, Waltham, MA 02453, USA

*: Corresponding author (email: turrigiano@brandeis.edu)

ABSTRACT

Sleep is widely believed to be an essential regulator of synaptic plasticity, but there is disagreement on whether it primarily enables correlation-based plasticity mechanisms such as long-term potentiation (LTP), or homeostatic forms of plasticity. Notably, it has been postulated that patterns of brain activity during sleep induce a widespread homeostatic downscaling of excitatory synaptic strengths across the brain. Here we use a combination of real-time sleep classification, *ex vivo* measurements of postsynaptic strength, and *in vivo* optogenetic monitoring of thalamocortical synapses in primary visual cortex (V1) to ask whether sleep and wake states can constitutively drive synaptic plasticity within neocortical circuits. We found that miniature EPSCs onto L4 or L2/3 pyramidal neurons were stable across sleep and wake dense epochs in both V1 and prefrontal cortex (PFC). Further, chronic monitoring of thalamocortical synaptic efficacy in V1 of freely behaving animals revealed remarkable stability of thalamocortical transmission across prolonged natural sleep and wake epochs. Together these data provide strong evidence against the view that sleep drives widespread constitutive weakening of excitatory synaptic strengths.

INTRODUCTION

Sleep is a widely expressed behavior, present in animals as evolutionarily distant as Cassiopea jellyfish and the Australian dragon lizard (Nath et al., 2017; Idelson et al., 2016). Despite its ubiquity and long history of scientific study, sleep – and more broadly the function of brain states – remains deeply mysterious. Sleep disruption can perturb learning and memory consolidation (Walker and Stickgold, 2004; Krause et al., 2017), presumably through the modulation of synaptic plasticity (Frank and Cantera, 2014). However, there is little agreement on the nature of this regulation. Researchers have variously proposed that sleep stabilizes, strengthens, weakens, or even prunes synapses (Kavanau, 1996; Datta et al., 2008; de Vivo et al., 2017; Li et al., 2017). Further, there is disagreement on whether sleep primarily enables correlation-based plasticity mechanisms such as long-term potentiation (LTP), or homeostatic forms of plasticity that serve the function of regulating overall synaptic strength to stabilize neuron and circuit function (Frank and Cantera, 2014, Aton et al., 2014; Hengen et al., 2016). Finally, it is unclear whether sleep is merely permissive for some forms of synaptic

bioRxiv preprint doi: https://doi.org/10.1101/829234; this version posted November 4, 2019. The copyright holder for this preprint (which was not certified by peer review) is the author/funder. All rights reserved. No reuse allowed without permission.

plasticity, or whether being asleep is by itself sufficient to induce synaptic changes without a preceding salient learning event (Tononi and Cirelli, 2014). Here we use a combination of real-time sleep classification, *ex vivo* measurements of postsynaptic strength, and *in vivo* optogenetic monitoring of thalamocortical synapses in primary visual cortex (V1) to ask whether sleep and wake states can constitutively drive synaptic plasticity within neocortical circuits.

One influential hypothesis, the synaptic homeostasis hypothesis (SHY), has motivated much work on the role of sleep in brain plasticity (Tononi and Cirelli, 2014). SHY proposes that memories are formed during wake when animals actively sample their environment, primarily through the induction of Hebbian LTP-like mechanisms that causes a net potentiation of synapses. This process would saturate synapses if left unopposed (Miller and MacKay, 1994; Abbott and Nelson, 2000; Turrigiano and Nelson, 2004), and sleep is proposed to be an offline state that allows neurons to renormalize synaptic weights by downscaling synaptic strengths (Tonoi and Cirelli, 2014). This renormalization is postulated to be a global process that affects all or most synapses in many brain regions (Tononi and Cirelli, 2014). Critically, SHY predicts that excitatory synapses should on average be stronger after a period of wake, and weaker after a period of sleep. In support of SHY some studies have found that the expression of proteins associated with synaptic potentiation are higher, axon-spine interfaces (a corollary of synaptic strength) are larger, and evoked transcallosal cortical responses increase in amplitude after a period of wake (Vyazovksiy et al., 2008; de Vivo et al., 2017; Diering et al., 2017). Importantly, these changes were observed under basal conditions, suggesting that simply being asleep or awake reduces or increases net synaptic weights (respectively), regardless of the prior experience of the animal. On the other hand, chronic long-term monitoring of firing rates as animals underwent natural sleep and wake episodes revealed no change in firing rates during extended periods of sleep or wake (Hengen et al., 2016), as one would expect if excitatory synapses are oscillating in strength.

Together, these studies paint a complex picture of the possible roles of sleep and wake states in modulating synaptic plasticity. Some discrepancies between studies are likely due to methodological differences; for instance some studies did not clearly differentiated between effects of sleep and circadian cycle, did not carefully classify sleep states and prior sleep history, or only indirectly measured synaptic strengths. Here we designed a direct test of the hypothesis that synaptic weights weaken during sleep and strengthen during wake, using both *ex vivo* slice physiology and *in vivo* monitoring of synaptic strengths. We used *in vivo* behavioral state classification in real time to track the accumulation of sleep and wake, which allowed us to detect natural sleep or wake-dense epochs that occurred within a defined 8 hour circadian window (ZT 0-8). We then immediately cut slices and measured miniature excitatory postsynaptic currents (mEPSCs) from pyramidal neurons in V1 or prefrontal cortex (PFC; specifically, prelimbic and infralimbic cortex). We found that mEPSCs were stable across sleep and wake dense epochs in both brain regions. To verify this finding, we used *in vivo* optogenetics to monitor thalamocortical synaptic drive to visual cortex across natural sleep-wake epochs. Again, we found that thalamocortical synaptic drive was stable across periods of sleep and wake. Together our data show that synaptic strengths are remarkably stable during naturally occurring periods of sleep and wake, and provide strong evidence against the view that a universal function of sleep is to drives widespread constitutive weakening of synaptic strengths.

bioRxiv preprint doi: https://doi.org/10.1101/829234; this version posted November 4, 2019. The copyright holder for this preprint (which was not certified by peer review) is the author/funder. All rights reserved. No reuse allowed without permission.

RESULTS

Real-time sleep classification

In order to directly assess synaptic strengths after sleep and wake, we designed an *in vivo* recording paradigm that performs behavioral state classification in real time. Briefly, we collect EEG, EMG from the nuchal (neck) muscles, and video from juvenile rats (P25-P31) as they freely behave in a chamber. The data were acquired, analyzed, and plotted all within a custom MATLAB program, which uses canonical markers to classify behavioral state into NREM, REM, or wake (Fig. 1A). Briefly, the program computes a delta/beta and a theta/delta ratio from the corresponding frequency bands in the EEG (delta: 0.5-4 Hz; theta: 5-8 Hz; beta ~ 20-35 Hz). Large deflections in the EMG are normalized and animal pixel movement is extracted from the video recording. The classifier reads in these variables and applies a simple semi-automated decision tree, which uses 3 manually adjustable thresholds (delta, theta, and movement thresholds). The classifier then adjusts these thresholds based on recent state history. With this technique, we can pull out highly differentiable states and achieve an accuracy of roughly 94% when benchmarked against manual coding (Fig. 1C). All classifications made in real time can be manually verified post hoc.

This real time behavioral state classifier greatly improved our ability to explore the effects of sleep on synaptic strengths, because rodent sleep is both highly variable and fragmented (Fig. 1A; see standard deviation Fig. 2A). While Long-Evans rats tend to sleep more during the day and are more active during the night, their hourly behavior is far more complex. A given animal might experience a sleep dense episode during the night and a wake dense one during the day (Fig. 2B); on average, the chance of being in a sleep dense epoch between ZT 0-4 was less than 50% (Fig. 2B), indicating that circadian time is not a good predictor of sleep history for individual animals. While inter-animal variability was high, we found that variation within an animal (between days) was significantly lower, allowing better prediction of future sleep states. We defined sleep/wake dense epochs as 4 hr. >65% in state (similar to previous studies; Liu et al., 2010; Hengen et al., 2016); using real time classification we were able to precisely identify such sleep or wake dense epochs within the first 8 hours at the start of the light period. To increase the probability of capturing a wake dense epoch, animals were encouraged to stay awake by giving them new toys at the end of a long natural wake period. Further, we set our criteria such that the last hour had to be especially sleep or wake enriched (>70% in state), to remove the possibility that synaptic differences might be rapidly reversed by behavioral state changes.

Postsynaptic strengths are stable across extended periods of sleep or wake

In order to directly test the impact of sleep on synapses, we tracked sleep/wake history in real time, and performed patch electrophysiology in acute slices once an animal experienced a sleep or wake dense period (Fig. 1B). We decided to employ *ex vivo* slice physiology as it is an established method to probe experience-dependent changes in synaptic strengths (Khurana and Li, 2013; Lambo and Turrigiano, 2013; Nataraj et al., 2010; Heynan et al., 2003; Nate Miska et al., 2018). To measure the postsynaptic strengths of many synapses onto individual neurons, we recorded mEPSCs from pyramidal cells in two different cortical regions and layers. We first looked at pyramidal neurons in layer 4 of primary visual cortex. These neurons receive extensive input from thalamic relay neurons, which vary their firing patterns dramatically during sleep

bioRxiv preprint doi: https://doi.org/10.1101/829234; this version posted November 4, 2019. The copyright holder for this preprint (which was not certified by peer review) is the author/funder. All rights reserved. No reuse allowed without permission.

(Steriade, 2001; Steriade and Timofeev, 2003), suggesting that if sleep-dependent changes in synaptic strength occur this might be a good place to look. In contrast to the prediction of SHY, mEPSC amplitudes were indistinguishable after wake dense or sleep dense epochs, both for cell means (Fig. 3D) and for cumulative amplitude distributions (Fig. 3E). We next recorded from layer 2/3 pyramidal neurons in primary visual cortex, as we have previously detected changes in mEPSC amplitude during experience-dependent plasticity in these neurons (Lambo et al., 2013; Hengen et al., 2013). As for L4 pyramidal neurons, mEPSC amplitudes in L2/3 pyramidal neurons were identical after wake dense or sleep dense epochs (Fig. 3B,C). To determine whether this stability was confined to primary sensory cortex, we next examined mEPSCs from L2/3 pyramidal neurons in PFC, where a previous study found weaker synapses after sleep (Liu et al., 2010). Consistent with our findings in primary visual cortex, mEPSC amplitude was also stable across sleep and wake dense epochs in PFC (Fig. 3F,G). MEPSC kinetics and passive cellular properties were not different for any condition. As expected, the frequency of mEPSC events was more variable between cells than was amplitude (Lambo et al., 2013; Hengen et al., 2013; Liu et al., 2010), and no significant differences were found in mean mEPSC frequency across conditions (Fig. S1). Cumulative distributions of inter-event intervals revealed only minor differences between conditions that were not consistent across brain areas (Fig. S1).

We wondered whether circadian time might impact postsynaptic strengths independently of sleep/wake history. To test this, we entrained animals to an inverted light/dark cycle, and then sacrificed them after a natural wake-dense period within the first 8 hr. of the dark cycle (such that slicing and recording was performed during the day for the experimenter). We found that mean mEPSC amplitude was similar across circadian time for both V1 and PFC (Fig. 3B,F, inverted wake), with only minor shifts in the cumulative amplitude distribution (Fig. 3C,G). Thus, circadian cycle has a subtle impact on the postsynaptic strength of excitatory synapses, that is independent of sleep history. Together, these acute slice recordings suggest a remarkable stability of postsynaptic strengths across sleep/wake and circadian cycle.

Thalamocortical evoked field potentials are stable over the course of sleep and wake

MEPSCs directly measure the distribution of postsynaptic strengths onto individual neurons, but a limitation of patch physiology is that it does not easily permit multiple measurements in a single animal over the course of sleep and wake epochs. To complement the mEPSC measurements we therefore designed a paradigm to measure neuronal responses continuously *in vivo* across sleep and wake epochs in a single freely behaving animal. In order to evoke synaptic responses in visual cortex from a defined population of inputs we took advantage of our ability to express ChR2 in thalamocortical terminals within V1 (Miska et al., 2018) by virally expressing ChR2 (AAV-ChR2-mCherry) in dorsal lateral geniculate nucleus (dLGN) of the thalamus, which projects extensively to layer 4 of V1. Injected animals were given 1.5-2 weeks to allow for expression and transport of ChR2 to axon terminals in V1 (Fig. 4A), at which time we implanted linear 16 channel silicon probes (NeuroNexus) into V1 with adhered optic fibers (ThorLabs, Doric Lenses) that rested on the cortical surface. We could reliably evoke thalamocortical responses with 1-2 ms pulses of blue light in these freely behaving animals (Fig. 4B-E). The linear design of the probe with exact electrode spacing, combined with current-source density analysis (Fig. 4B) and post hoc histology, allowed us to estimate the placement of electrical sites with high confidence. The thalamic stimulation evoked responses similar to those evoked by

bioRxiv preprint doi: https://doi.org/10.1101/829234; this version posted November 4, 2019. The copyright holder for this preprint (which was not certified by peer review) is the author/funder. All rights reserved. No reuse allowed without permission.

electrical stimulation of LGN, as well as visually evoked potentials (Cooke and Bear, 2010; Niell and Stryker, 2008). The amplitude of the first negative trough of this field excitatory postsynaptic potential (fEPSP) arises from monosynaptic thalamic connections onto V1 neurons (Cooke and Bear, 2010).

To chronically monitor the amplitude of thalamocortical fEPSPs, we chose light intensities below the peak saturation of responses (normally ~50% of the peak response), and very low stimulation frequencies (1/20 - 1/40 Hz) to avoid inducing plasticity from the stimulation itself. With these parameters we were able to measure stable cortical responses to thalamic stimulation continuously for up to several days (Fig. 4E), while monitoring the sleep/wake state of the animal. An interesting feature of these recordings is that the size of fEPSP varied strongly between behavioral states (Fig. 4E). Evoked potentials were larger on average during NREM than wake, while events during REM were intermediate in size. These differences between states manifested rapidly upon state changes, consistent with a rapid neuromodulatory effect on the efficacy of thalamocortical synapses (Lee and Dan, 2012; Brown et al., 2012). Because of these amplitude differences between states, we designed a "sandwich" method for detecting changes across prolonged periods of sleep, by examining periods of extended sleep with flanking periods of wake. We then measured the normalized change in amplitude between these two wake periods to determine the impact of the intervening period of sleep (Fig. 5a). Using this sandwich approach we found that fEPSPs amplitudes were stable across periods of sleep and wake (Fig. 5b,c), indicating that sleep and wake produce no persistent changes in synaptic strength. SHY predicts that sleep should produce a gradual decrease in the size of the fEPSPs, that should be proportional to the amount of sleep (Vyazovskiy et al., 2008). To take advantage of the continuous sampling in these experiments, we next measured how the fEPSP amplitudes changed over the course of periods of sleep or wake (Fig. 5D). This analysis revealed the rapid change in fEPSP amplitude immediately upon state change, with a decrease at the transition from sleep to wake and vice-versa (Fig. 5E); however, fEPSP amplitude remained stable after this, with no progressive change in amplitude across either sleep or wake states (Fig. 5e). Taken together with our mEPSC data, these experiments reveal that neocortical synaptic weights are stable across extended periods of sleep and wake.

Thalamocortical evoked firing rates are stable over the course of sleep and wake

Although thalamocortical fEPSP amplitudes were not modulated by time awake or asleep, it is possible that the ability of thalamocortical synapses to evoke spiking in postsynaptic V1 neurons could be modified by prolonged periods of sleep or wake. In addition to recording fEPSPs, our optrodes allowed us to sample spikes in V1 evoked by stimulation of thalamocortical inputs (Fig. 6A). Using spike sorting as described (Hengen et al., 2016), we were able to follow spiking in individual neurons over the course of sleep and wake epochs as for fEPSPs (Fig. 6B). Similar to our previous findings (Hengen et al., 2016; Torrado Pacheco et al., 2019b), we saw only small (and not statistically significant) difference in mean spontaneous firing rates between sleep and wake states, or across extended sleep or wake epochs.

Next, we set out to determine whether evoked spiking was affected by prolonged periods of sleep or wake. Most well-isolated units had a detectable response to the thalamocortical stimulation (Fig. 6D). When we analyzed the evoked firing during different brain states, we found (consistent with the fEPSP responses) that spiking responses were larger on average during

bioRxiv preprint doi: https://doi.org/10.1101/829234; this version posted November 4, 2019. The copyright holder for this preprint (which was not certified by peer review) is the author/funder. All rights reserved. No reuse allowed without permission.

NREM, intermediate during REM, and smaller during wake (Fig. 6B). To determine whether evoked firing changed as a result of time spent asleep or awake, we again used the sandwich method (Fig. 6C,D) to compare the magnitude of evoked firing before and after sleep or wake dense epochs. We found no significant differences in evoked responses after intervening periods of sleep or wake (Fig. 6D,E). Taken in concert with the fEPSP results, this shows that time spent asleep does not cause persistent changes in the efficacy of thalamocortical synaptic transmission.

DISCUSSION

It has been postulated that patterns of brain activity during sleep induce a widespread downscaling of excitatory synaptic strengths throughout many CNS circuits, but the evidence for this has been contradictory. Here we used real-time sleep classification in freely behaving animals to carefully disentangle circadian from sleep effects, and then used *ex vivo* electrophysiology and *in vivo* optogenetics to ask whether simply being asleep is able to constitutively drive synaptic weakening. We found that mEPSCs onto L4 or L2/3 pyramidal neurons were stable across sleep and wake dense epochs in both V1 and PFC. Further, chronic monitoring of thalamocortical synaptic efficacy in V1 of freely behaving animals revealed remarkable stability of thalamocortical transmission across prolonged natural sleep and wake epochs. Together these data provide strong evidence against the view that sleep drives widespread constitutive weakening of excitatory synaptic strengths.

Several previous studies have reported that molecular or morphological correlates of synaptic strength are lower after a period of sleep than a period of wake (Vyazovksiy et al., 2008; de Vivo et al., 2017; Diering et al., 2017). There are several methodological differences between our approach and previous studies that might explain these differences. First, we rigorously classified the sleep history of every animal used for our *ex vivo* recordings, rather than relying on video classification of sleep history, which is considerably less accurate. Second, we carefully controlled for circadian time, which has often been used as a proxy for sleep and wake despite the potential impact of circadian time itself on synaptic strengths (Diering et al., 2017; discussed in Frank and Cantera, 2014), and the considerable variability across individual animal in sleep habits. Our data show, for example, that in these ~4 week old animals, the chance of having experienced a sleep dense epoch at ZT 4 or 6 (time points used in many studies) is < 50%. Third, we used direct electrophysiological measurements of synaptic strength across natural sleep and wake cycles, whereas many studies have relied on sleep deprivation paradigms to manipulate the amount of sleep, or used indirect measures of synaptic function as proxies for synaptic strength (Vyazovksiy et al., 2008; Liu et al., 2010). Finally, several studies reporting correlates of synaptic weakening after sleep have looked in motor cortex (Vyazovksiy et al., 2008; de Vivo et al., 2017; Diering et al., 2017), whereas here we examined synaptic strengths in visual and prefrontal cortex, raising the possibility that the impact of sleep on synaptic function may be distinct in different brain areas. Regardless, our data show that synaptic downscaling is not a universal function of sleep across cell types and brain regions.

Using a direct measure of postsynaptic strength, we found that mEPSC amplitude was stable across sleep and wake epochs in three cell types from two very different cortical areas. These findings are inconsistent with a previous study that reported that mEPSCs in frontal cortex

bioRxiv preprint doi: https://doi.org/10.1101/829234; this version posted November 4, 2019. The copyright holder for this preprint (which was not certified by peer review) is the author/funder. All rights reserved. No reuse allowed without permission.

(including the PFC region we recorded from in this study) were smaller and less frequent after a period of sleep than after a period of sleep deprivation (Lui et al., 2010). While there are a number of possible explanations for this discrepancy, one major difference is that here we more carefully controlled for sleep history in individual animals. A second major difference is that we recorded from defined cell types and layers within well-defined brain regions, whereas the previous study sampled from several distinct regions and did not report cell type; as mEPSC frequency and amplitude can vary considerably between cell types, these measures could be strongly affected by sampling differences between conditions. An important question is whether mEPSC measurements are sensitive enough to detect changes in synaptic strength induced by 4 hours of consolidated sleep or wake. We have used a similar approach to successfully quantify changes in mEPSC amplitude induced by visual deprivation, and can reliably detect both increases and decreases of <10% with a similar sample size to the present study. Previously reported changes in synaptic parameters following sleep are larger than that (De Vivo et al., 2017), suggesting that if they were occurring at these synapses we would have been able to detect them.

In addition to measuring mEPSC amplitude *ex vivo*, we also devised an approach that let us follow optogenetically-evoked thalamocortical synaptic inputs over long periods of time in freely behaving animals, so that we could follow changes in strengths at a defined set of synaptic inputs in real time during naturally occurring periods of extended sleep or wake. Consistent with our mEPSC recordings, we found that these evoked synaptic inputs were remarkably stable during sleep and wake. One concern with this approach is that repeated optogenetic measurements from the same synapses might itself affect the synaptic responses. However, under our stimulation conditions we were able to evoke consistent and stable responses over several days, suggesting that we were not inducing significant phototoxicity or synaptic plasticity. Blue light stimulation by itself can affect neuronal health and RNA expression (Tyssowski and Gray, 2019), but here we used lower light intensities and very low stimulation frequencies (1/20 to 1/40 Hz), so total exposure to blue light was ~300 X less per hour than what has been shown to impair neuronal health.

Interestingly, we found that the evoked thalamocortical fEPSP responses were rapidly modulated by transitions between brain state as has been briefly described before using different paradigms (Vyazovskiy et al., 2008; Reinhold et al., 2015; Hall and Borbely, 1970). These state-dependent transitions might be due to changes in neuromodulatory tone (Lee and Dan, 2012), and/or changes in the network activity in the thalamus or V1 (Steriade, 2001; Steriade and Timofeev, 2003) between sleep and wake states. This increase in the evoked synaptic component of the responses also translated into an enhanced ability to evoke spikes in V1 neurons, suggesting that thalamic responses in cortex are amplified when the animal is in NREM sleep. This response amplification might have interesting implications for information transfer during sleep.

Taken together our data show that simply being awake or asleep is not sufficient to induce widespread increases or decreases in cortical synaptic strengths. This is consistent with data from V1 showing that firing rates are not modulated by time spent asleep or awake (Hengen et al., 2016; Torrado Pacheco et al., 2019b). On the other hand, there is a large body of work showing that sleep and wake states can profoundly affect the induction of various forms of plasticity when they are initiated by robust learning or sensory deprivation paradigms. For

bioRxiv preprint doi: https://doi.org/10.1101/829234; this version posted November 4, 2019. The copyright holder for this preprint (which was not certified by peer review) is the author/funder. All rights reserved. No reuse allowed without permission.

example, sleep facilitates and is required for ocular dominance plasticity, and roles for NREM and REM sleep have been found in promoting growth, maintenance, and loss of specific synaptic connections during learning (Frank et al., 2001; Chauvette et al., 2012; Yang et al., 2014; Li et al., 2017). In addition, when firing in V1 is perturbed using visual deprivation/restoration paradigms to induce homeostatic compensation, upward firing rate homeostasis is confined to periods of active wake (Hengen et al., 2016), while downward firing rate homeostasis is confined to periods of sleep (Torrado Pacheco et al., 2019). It thus seems likely that sleep does not have a single unified constitutive effect on synaptic strengths, but rather that sleep and wake states are able to gate the induction of various forms of synaptic plasticity when they are induced by salient learning events, or dramatic changes in sensory experience (Frank and Cantera, 2014).

bioRxiv preprint doi: https://doi.org/10.1101/829234; this version posted November 4, 2019. The copyright holder for this preprint (which was not certified by peer review) is the author/funder. All rights reserved. No reuse allowed without permission.

METHODS

Overview

All experiments were performed on Long-Evans rats of both sexes between postnatal day P25 and 31. Litters were housed on a 12:12 light cycle with the dam with free access to food and water. All animals were housed, cared for, surgerized, and sacrificed in accordance with Brandeis IBC and IACAUC protocols.

Virus injections into dLGN

Viral injections were performed between P12-P16 using stereotaxic surgery under isoflurane anesthesia at 1.5-2.5%. Dorsal LGN was targeted bilaterally using stereotaxic coordinates after adjusting for the lambda-bregma distance for age. A glass micropipette pulled to a fine point delivered 400 nL of virus-containing solution at the targeted depth.

Electrode surgeries

Animals underwent electrode surgery at ages P21-P23. For animals to undergo acute slice physiology, we implanted 3 EEG screws (PlasticsOne): frontal lobe (B: +1-2, L: 1.5-2.5 mm), parietal lobe (B: -3-4, L: 1.5-2.5 mm), and cerebellum (for reference). In addition, two stainless steel spring electrodes were placed in the nuchal (neck) muscles of the rats for EMG recording. Screw electrodes were fed into a pedestal (PlasticsOne) and everything was secured with dental cement. For *in vivo* recording and stimulation experiments, a 16 channel silicon probe (Neuronexus) with adhered optic fiber (200-400 μm diameter; Doric Lenses or ThorLabs) were stereotaxically inserted into V1 in dLGN virus injected animals such that the fiber tip rested on the surface of the brain. In the majority of these surgeries light stimulation and sample recording were performed during the operation in order to verify correct placement of the electrode and expression of the virus. Exposed craniotomy was surrounded with a silicone elastomer (Kwik-Cast, World Precision Instruments, Sarasota, FL, USA). The array was secured using dental cement, then grounded to two screws (cerebellum and frontal lobe) using steel wire and soldering paste. Animals were given 2-3 days of recovery before data collection.

Real time behavioral recording and classification

Animals with EEG/EMG head caps were connected to a flexible cable and low resistance commutator (PlasticsOne). The signal was amplified and filtered with BioPac EEG and EMG amplifiers at x5000 and x500, respectively. This analog signal was then digitized with a NIDAQ board (National Instruments). The data were acquired, analyzed, and plotted all within a custom MATLAB program, which uses canonical markers to classify behavioral state as either: NREM, REM, or wake. Briefly, the program computes a delta/beta and a theta/delta ratio from the corresponding frequency bands in the EEG (delta: 0.5-4 hz; theta: 5-8 hz; beta ~ 20-35 hz). Large deflections in the EMG are normalized and animal pixel movement is extracted from the video recording (infrared light allowed following the animal in darkness). The program uses 3 manually adjustable thresholds (delta, theta, and movement thresholds),which are additionally adjusted given recent behavioral states. The classifier uses the EEG ratios and movement measures and applies a decision tree which predicts states in 10 second epochs given the thresholds. The recent behavioral data is plotted and added to a graph that contains the full behavioral history of the animal. This cycle repeats every 4 mins.

bioRxiv preprint doi: https://doi.org/10.1101/829234; this version posted November 4, 2019. The copyright holder for this preprint (which was not certified by peer review) is the author/funder. All rights reserved. No reuse allowed without permission.

Ex vivo acute brain slice preparation

For brain slice preparation, animals between P25 and P31 were briefly anesthetized with isoflurane (usually under 60 seconds), and coronal brain slices (300 μm) containing V1 or prefrontal cortex were obtained from both hemispheres of each animal. After slicing in carbogenated (95% O_2, 5% CO_2) standard ACSF (in mM: 126 NaCl, 25 $NaHCO_3$, 3 KCl, 2 $CaCl_2$, 2 $MgSO_4$, 1 NaH_2PO_4, 0.5 Na-Ascorbate, osmolarity adjusted to 315 mOsm with dextrose, pH 7.35), slices were immediately transferred to a warm (34°C) chamber filled with a continuously carbogenated 'protective recovery' (Ting et al., 2014) choline-based solution (in mM: 110 Choline-Cl, 25 $NaHCO_3$, 11.6 Na-Ascorbate, 7 $MgCl_2$, 3.1 Na-Pyruvate, 2.5 KCl, 1.25 NaH_2PO_4, and 0.5 $CaCl_2$, osmolarity 315 mOsm, pH 7.35) for 10 min, then transferred back to warm (34°C) carbogenated standard ACSF and incubated another 20-30 min. Slices were used for electrophysiology between 1 – 6 hr. post-slicing.

Whole cell recordings

V1 and prefrontal cortex were identified in acute slices using the shape and morphology of the white matter as a reference. Pyramidal neurons were visually targeted and identified by the presence of an apical dendrite and teardrop shaped soma, and morphology was confirmed by *post hoc* reconstruction of biocytin fills. Borosilicate glass recording pipettes were pulled using a Sutter P-97 micropipette puller, with acceptable tip resistances ranging from 3 to 5 MΩ. Cs+ Methanesulfonate-based internal recording solution was modified from Xue et al., 2014, and contained (in mM) 115 Cs-Methanesulfonate, 10 HEPES, 10 BAPTA•4Cs, 5.37 Biocytin, 2 QX-314 Cl, 1.5 $MgCl_2$, 1 EGTA, 10 Na_2-Phosphocreatine, 4 ATP-Mg, and 0.3 GTP-Na, with sucrose added to bring osmolarity to 295 mOsm, and CsOH added to bring pH to 7.35. Inclusion criteria included V_m, R_{in}, and R_s cut-offs as appropriate for experiment type and internal solution; values are listed below.

All recordings were performed on submerged slices, continuously perfused with carbogenated 34°C recording solution. Neurons were visualized on an Olympus upright epifluorescence microscope using a 10x air (0.13 numerical aperture) and 40x water-immersion objective (0.8 numerical aperture) with infrared-differential interference contrast optics and an infrared CCD camera. Data were low-pass filtered at 5 kHz and acquired at 10 kHz with Axopatch 200B amplifiers and CV-7B headstages (Molecular Devices, Sunnyvale CA). Data were acquired using an in-house program written either in Igor Pro (Wavemetrics, Lake Oswego OR) or MATLAB (Mathworks, Natick MA), and all post-hoc data analysis was performed using in-house scripts written in MATLAB (Mathworks, Natick MA).

mEPSC recordings

For spontaneous mEPSC recordings, pyramidal neurons were voltage clamped to −70 mV in standard ACSF containing a drug cocktail of TTX (0.2 μM), APV (50 μM), picrotoxin (25 μM). 10 s traces were obtained and amplified (10-20x). Event inclusion criteria included amplitudes greater than 5 pA and rise times less than 3 ms. Neurons were excluded from analysis if $R_s > 25$ MΩ or $V_m > -50$ mV.

mEPSC analysis

In order to both reliably detect mEPSC events above noise and to limit bias in selection, we used an in-house program written in MATLAB that employs a semi-automated template-based

bioRxiv preprint doi: https://doi.org/10.1101/829234; this version posted November 4, 2019. The copyright holder for this preprint (which was not certified by peer review) is the author/funder. All rights reserved. No reuse allowed without permission.

detection method contained in a GUI. In brief, the program first filters the raw current traces and then applies a canonical mEPSC event shaped template to detect regions of best fit. Multiple tunable parameters for template threshold and event kinetics that aid in detection were optimized and then chosen to stay constant for all analyses. Putative events are then analyzed for hallmark features of mEPSC (risetime kinetics, decay time, minimum amplitude cutoffs, etc.). Finally, the results of the automated detection are reviewed manually; <5% automatically detected events were excluded, and <5% of total events were missed by detection and manually added.

Array recording and stimulation

During the few days before recording, animals were handled twice daily by the experimenter. The day before recording started animals were transferred to a clear plexiglass cage of dimensions 12”x12”x16” (length, depth, height) and separated into two arenas by a clear plastic divider with 1” holes to allow for tactile and olfactory interaction while preventing aggressive play and jostling of headcaps. Animals were kept on a 12h/12h light/dark cycle in a temperature- and humidity-controlled room (21ºC, 25-55% humidity). The arrays were connected to an Intan RHD2216 amplifier board, which in turn was connected to a RHD2000 SPI interface cable (Intan). The cable connected to a custom designed Hall effect-based active commutator (NeuroTek Innovative Technology Incorporated; Toronto, Ontario, Canada). The commutator fed this digitized data into the RHD2000 USB board (Intan). Data were recorded at 25 kHz continuously for up to 100 hours using the RHD2000 Interface Software (Intan). Spike extraction, clustering and sorting were done using custom Matlab and Python code (see below).

Semi-automated spike extraction, clustering and sorting

Spike extraction clustering and sorting was performed as previously described (Hengen et al., 2016; Torrado Pacheco, Tilden, Grutzner et al., 2019). Spikes were detected in the raw signal as threshold crossings (-4 standard deviations from mean signal) and re-sampled at 3x the original rate. Principal component analysis (PCA) was done on all spikes from each channel, and the first four principal components were used for clustering (Harris et al., 2000). A random forest classifier implemented in python was used to classify spikes according to a model built on a dataset of 1200 clusters manually scored by expert observers. A set of 19 features, including ISI contamination (% of ISIs < 3 msec), similarity to regular spiking unit (RSU) and fast-spiking unit (FS) waveform templates, amount of 60 Hz noise contamination and kinetics of the mean waveform. Cluster quality was also ensured by thresholding of L-ratio and isolation distance (Schmitzer-Torbert et al., 2005). Clusters were classified as noise, multi-unit or single-unit. Only single-unit clusters with a clear refractory period were used for FR analysis. We classified units as RSU or FS based on established criteria (mean waveform trough-to-peak and tail slope, Hengen et al., 2016). Only RSUs (putative excitatory neurons) were used for analysis. Many neurons were lost during the recording, presumably due to electrode drift or gliosis. To establish “on” and “off” times for neurons, we used ISI contamination: when hourly % of ISIs < 3 msec was above 4%, unit was considered to be offline. Results of the automated scoring were manually reviewed for final inclusion of units.

Post hoc semi-automated behavioral state scoring

In order to perform the final classification of behavior after experiments an in-house MATLAB/Python GUI was used. The GUI uses the same features and decision tree for real time classification in for the first several hours of data, which is manually reviewed for accuracy. A

bioRxiv preprint doi: https://doi.org/10.1101/829234; this version posted November 4, 2019. The copyright holder for this preprint (which was not certified by peer review) is the author/funder. All rights reserved. No reuse allowed without permission.

200-300 tree random forest machine learning algorithm is trained on this initial part of the recording for each animal. It is given the same features as for automated classification, but with additional features found to be useful for the decision tree. These included: the proportional contribution of delta, theta, and gamma powers; min/max EEG; and a past value of many of these features up to three 10 s bins ago. The random forest classifier was then applied and reviewed for the rest of the recording. Random forest accuracy was roughly 97% against manual coding.

Statistical analysis

All data analysis was performed using in-house scripts written in MATLAB (Mathworks, Natick MA). For each experiment, means ±SEM derived from individual cell measurements were provided within the results section of the text, and n's (number of cells and animals), P values, and statistical tests were provided within figure captions. A 2-sample t-test was used for normally distributed data, and a Wilcoxon rank sum test was used for data that were clearly not normally distributed. Lastly, a two-sample Kolmogorov-Smirnov test was used for comparisons between distributions. Data were considered significant if $p < 0.05$.

bioRxiv preprint doi: https://doi.org/10.1101/829234; this version posted November 4, 2019. The copyright holder for this preprint (which was not certified by peer review) is the author/funder. All rights reserved. No reuse allowed without permission.

REFERENCES

Abbott, L. F., & Nelson, S. B. (2000). Synaptic plasticity: taming the beast. *Nature Neuroscience*, *3*(november), 1178–1183. https://doi.org/10.1038/81453

Aton, S. J., Suresh, A., Broussard, C., & Frank, M. G. (2014). Sleep promotes cortical response potentiation following visual experience. *Sleep*, *37*(7), 1163–1170. https://doi.org/10.5665/sleep.3830

Brown, R. E., Basheer, R., McKenna, J. T., Strecker, R. E., & McCarley, R. W. (2012). Control of Sleep and Wakefulness. *Physiological Reviews*, *92*(3). https://doi.org/10.1152/physrev.00032.2011

Cooke, S. F., & Bear, M. F. (2010). Visual experience induces long-term potentiation in the primary visual cortex. *J Neurosci*, *30*(48), 16304–16313. https://doi.org/10.1523/JNEUROSCI.4333-10.2010

Datta, S., Li, G., & Auerbach, S. (2008). Activation of phasic pontine-wave generator in the rat: A mechanism for expression of plasticity-related genes and proteins in the dorsal hippocampus and amygdala. *European Journal of Neuroscience*, *27*(7), 1876–1892. https://doi.org/10.1111/j.1460-9568.2008.06166.x

de Vivo, L., Bellesi, M., Marshall, W., Bushong, E. A., Ellisman, M. H., Tononi, G., & Cirelli, C. (2017). Ultrastructural evidence for synaptic scaling across the wake/sleep cycle. *Science*, *355*(6324), 507–510. https://doi.org/10.1126/science.aah5982

Diering, G. H., Nirujogi, R. S., Roth, R. H., Worley, P. F., Pandey, A., & Huganir, R. L. (2017). Homer1a drives homeostatic scaling-down of excitatory synapses during sleep. *Science*, *515*(February), 511–515.

Frank, M. G., & Cantera, R. (2014). Sleep, clocks, and synaptic plasticity. *Trends in Neurosciences*, *37*(9), 491–501. https://doi.org/10.1016/j.tins.2014.06.005

Hall, R. D., & Borbely, A. A. (1970). Acoustically evoked potentials in the rat during sleep and waking. *Experimental Brain Research*, *11*(1), 93–110. https://doi.org/10.1007/BF00234203

Hengen, K. B., Lambo, M. E., VanHooser, S. D., Katz, D. B., & Turrigiano, G. G. (2013). Firing rate homeostasis in visual cortex of freely behaving rodents. *Neuron*, *80*(2), 335–342. https://doi.org/10.1016/j.neuron.2013.08.038

Hengen, K. B., Torrado Pacheco, A., McGregor, J. N., Van Hooser, S. D., & Turrigiano, G. G. (2016). Neuronal Firing Rate Homeostasis Is Inhibited by Sleep and Promoted by Wake. *Cell*, *165*(1), 1–12. https://doi.org/10.1016/j.cell.2016.01.046

bioRxiv preprint doi: https://doi.org/10.1101/829234; this version posted November 4, 2019. The copyright holder for this preprint (which was not certified by peer review) is the author/funder. All rights reserved. No reuse allowed without permission.

Heynen, A. J., Yoon, B. J., Liu, C. H., Chung, H. J., Huganir, R. L., & Bear, M. F. (2003). Molecular mechanism for loss of visual cortical responsiveness following brief monocular deprivation. *Nature Neuroscience*, *6*(8), 854–862. https://doi.org/10.1038/nn1100

Kavanau, J. L. (1996). Memory, sleep, and dynamic stabilization of neural circuitry: Evolutionary perspectives. *Neuroscience and Biobehavioral Reviews*, *20*(2), 289–311. https://doi.org/10.1016/0149-7634(95)00019-4

Khurana, S., & Li, W. (2013). Baptisms of fire or death knells for acute-slice physiology in the age of "omics" and light? *Rev. Neurosci.*, *24*(5).

Krause, A. J., Simon, E. Ben, Mander, B. A., Greer, S. M., Saletin, J. M., Goldstein-Piekarski, A. N., & Walker, M. P. (2017, July 1). The sleep-deprived human brain. *Nature Reviews Neuroscience*, Vol. 18, pp. 404–418. https://doi.org/10.1038/nrn.2017.55

Lambo, M. E., & Turrigiano, G. G. (2013). Synaptic and intrinsic homeostatic mechanisms cooperate to increase L2/3 pyramidal neuron excitability during a late phase of critical period plasticity. *The Journal of Neuroscience : The Official Journal of the Society for Neuroscience*, *33*(20), 8810–8819. https://doi.org/10.1523/JNEUROSCI.4502-12.2013

Lee, S. H., & Dan, Y. (2012). Neuromodulation of Brain States. *Neuron*, *76*(1), 109–222. https://doi.org/10.1016/j.neuron.2012.09.012

Li, W., Ma, L., Yang, G., & Gan, W.-B. (2017). REM sleep selectively prunes and maintains new synapses in development and learning. *Nature Neuroscience*, *20*(3). https://doi.org/10.1038/nn.4479

Liu, Z.-W., Faraguna, U., Cirelli, C., Tononi, G., & Gao, X.-B. (2010). Direct Evidence for Wake-Related Increases and Sleep-Related Decreases in Synaptic Strength in Rodent Cortex. *Journal of Neuroscience*, *30*(25), 8671–8675. https://doi.org/10.1523/JNEUROSCI.1409-10.2010

Miller, K. D., & MacKay, D. J. C. (1994). The Role of Constraints in Hebbian Learning. *Neural Computation*, *6*(1), 100–126. https://doi.org/10.1162/neco.1994.6.1.100

Miska, N. J., Richter, L. M. A., Cary, B. A., Gjorgjieva, J., & Turrigiano, G. G. (2018). Sensory experience inversely regulates feedforward and feedback excitation-inhibition ratio in rodent visual cortex. *ELife*, *7*. https://doi.org/10.7554/eLife.38846

Nataraj, K., Le Roux, N., Nahmani, M., Lefort, S., & Turrigiano, G. (2010). Visual deprivation suppresses L5 Pyramidal Neuron Excitability by Preventing the Induction of Intrinsic Plasticity. *Neuron*, *68*(4), 750–762. https://doi.org/10.1016/j.neuron.2010.09.033

Nath, R. D., Bedbrook, C. N., Abrams, M. J., Basinger, T., Bois, J. S., Prober, D. A., … Goentoro, L. (2017). The Jellyfish Cassiopea Exhibits a Sleep-like State. *Current Biology*, *27*(19), 2984-2990.e3. https://doi.org/10.1016/j.cub.2017.08.014

bioRxiv preprint doi: https://doi.org/10.1101/829234; this version posted November 4, 2019. The copyright holder for this preprint (which was not certified by peer review) is the author/funder. All rights reserved. No reuse allowed without permission.

Niell, C. M., & Stryker, M. P. (2008). Highly selective receptive fields in mouse visual cortex. *Journal of Neuroscience*, *28*(30), 7520–7536. https://doi.org/10.1523/JNEUROSCI.0623-08.2008

Pacheco, A. T., Bottorff, J., & Turrigiano, G. G. (2019). Sleep promotes downward firing rate homeostasis. *BioRxiv*, 827832. https://doi.org/10.1101/827832

Shein-Idelson, M., Ondracek, J. M., Liaw, H.-P., Reiter, S., & Laurent, G. (2016). Slow waves, sharp waves, ripples, and REM in sleeping dragons. *Science*, *352*(6285), 590–595. https://doi.org/10.1126/science.aaf3621

Ting, J. T., Daigle, T. L., Chen, Q., & Feng, G. (2014). Acute brain slice methods for adult and aging animals: application of targeted patch clampanalysis and optogenetics. *Methods in Molecular Biology (Clifton, N.J.)*, *1183*, 221. https://doi.org/10.1007/978-1-4939-1096-0_14

Tononi, G., & Cirelli, C. (2014). Sleep and the Price of Plasticity: From Synaptic and Cellular Homeostasis to Memory Consolidation and Integration. *Neuron*, *81*(1), 12–34. https://doi.org/10.1016/j.neuron.2013.12.025

Turrigiano, G. G., & Nelson, S. B. (2004). Homeostatic plasticity in the developing nervous system. *Nature Reviews. Neuroscience*, *5*(2), 97–107. https://doi.org/10.1038/nrn1327

Tyssowski, K. M., & Gray, J. M. (2019). Blue light induces neuronal-activity-regulated gene expression in the absence of optogenetic proteins. *BioRxiv*, 572370. https://doi.org/10.1101/572370

Vyazovskiy, V. V, Cirelli, C., Pfister-Genskow, M., Faraguna, U., & Tononi, G. (2008). Molecular and electrophysiological evidence for net synaptic potentiation in wake and depression in sleep. *Nature Neuroscience*, *11*(2), 200–208. https://doi.org/10.1038/nn2035

Walker, M. P., & Stickgold, R. (2004, September 30). Sleep-dependent learning and memory consolidation. *Neuron*, Vol. 44, pp. 121–133. https://doi.org/10.1016/j.neuron.2004.08.031

Xue, M., Atallah, B. V., & Scanziani, M. (2014). Equalizing excitation–inhibition ratios across visual cortical neurons. *Nature*, *511*(7511), 596–600. https://doi.org/10.1038/nature13321

bioRxiv preprint doi: https://doi.org/10.1101/829234; this version posted November 4, 2019. The copyright holder for this preprint (which was not certified by peer review) is the author/funder. All rights reserved. No reuse allowed without permission.

FIGURES

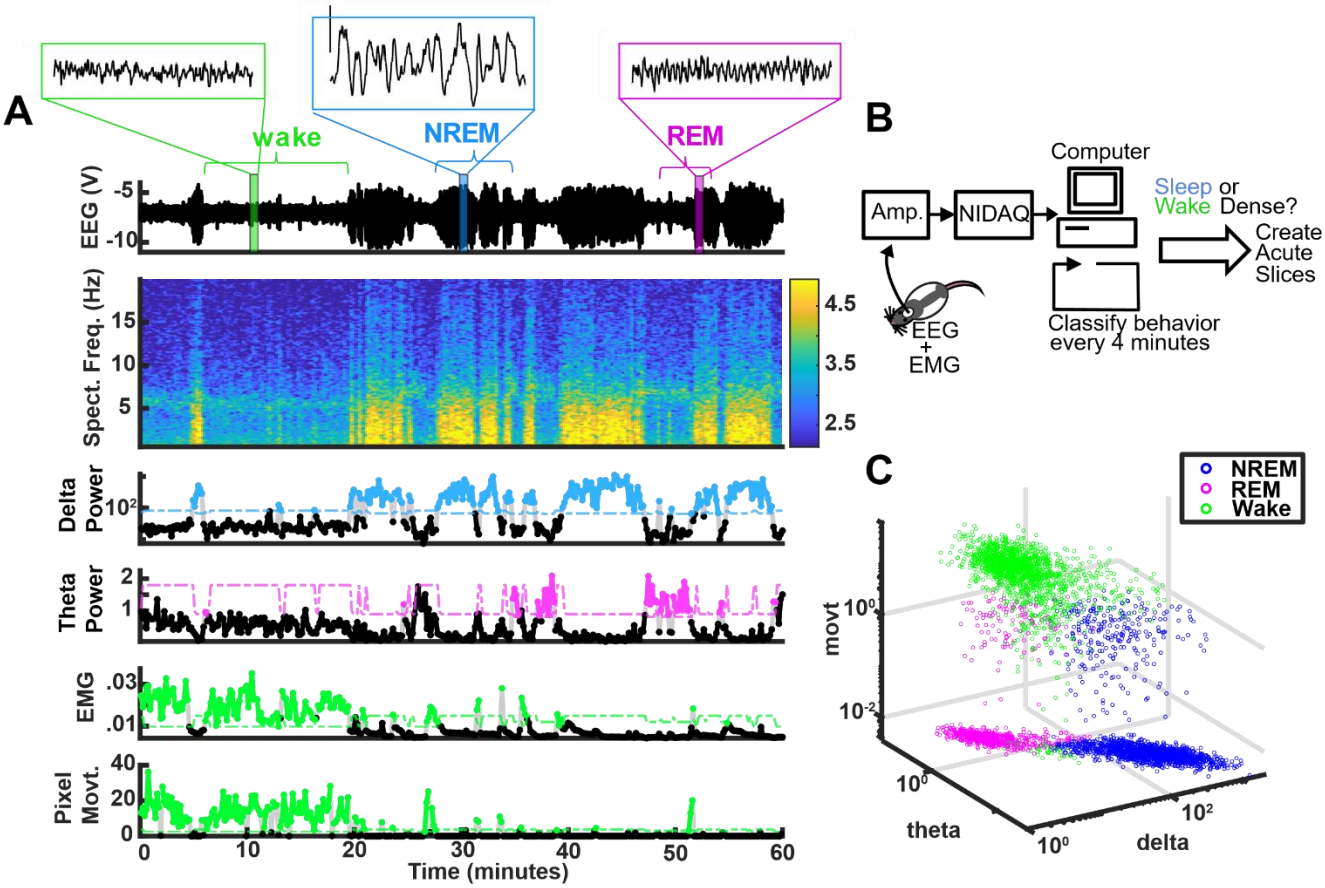

Figure 1. Behavioral state can be classified with high accuracy and in real time. (A) Here 1 hour of data is shown with relevant components for behavioral classification extracted. Top plot shows the raw EEG. Second, a spectrogram from 0-20 Hz colored by power. Third, delta/beta ratio. Fourth, theta/delta ratio. Fifth, normalized EMG deflection values. Sixth, animal movement in pixels as recorded with video. Component plots have an adjustable threshold for state classification plotted as dashed line; points above the threshold are shown as colored dots. **(B)** Schematic of real time classifier rig. **(C)** 3D plot of delta, theta, and movement measures (shown in A) colored by brain state; data from example animal.

bioRxiv preprint doi: https://doi.org/10.1101/829234; this version posted November 4, 2019. The copyright holder for this preprint (which was not certified by peer review) is the author/funder. All rights reserved. No reuse allowed without permission.

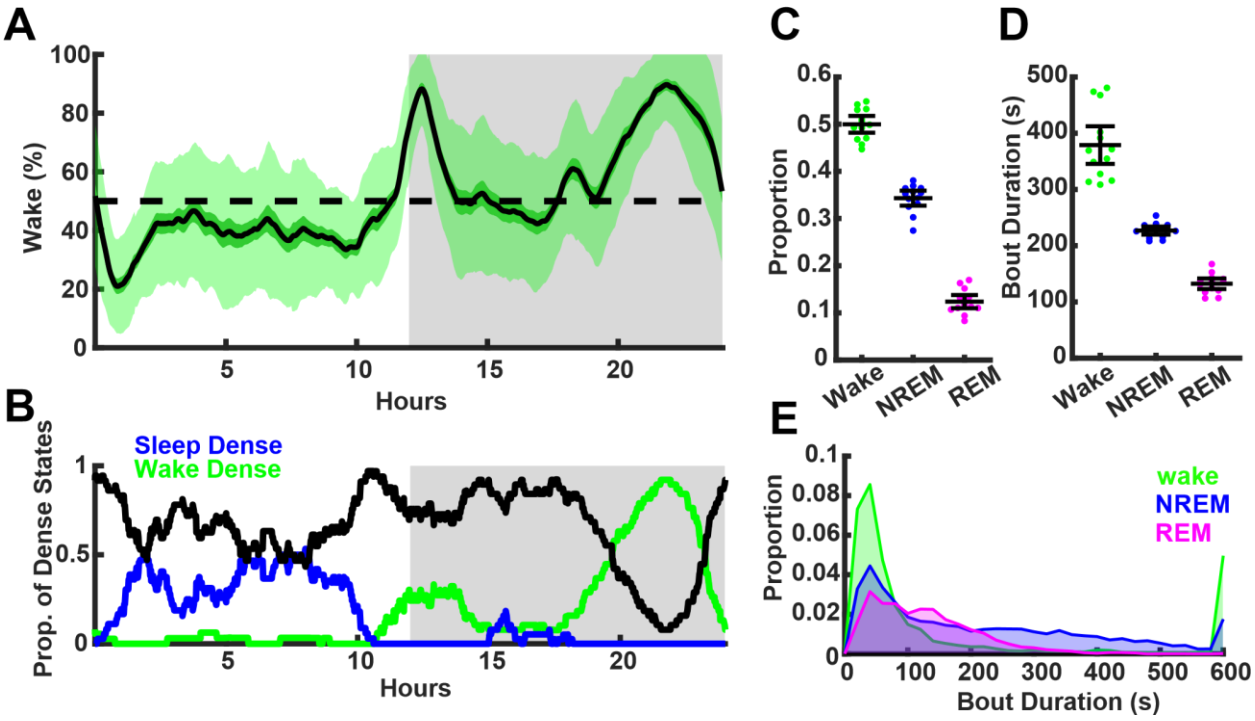

Figure 2. Sleep/wake behavior of juvenile rats. (A) Average wake percentage from total of 37 days of recording from 13 animals. Light shade = standard deviation; dark shade = SEM. **(B)** Probability of a given animal from (A) experiencing a >65% 4 hr. dense episode across the day; black line represents not dense episode probability. **(C)** Average bout duration of three behavioral states and **(D)** proportion of time spent in each state for each animal (n = 13). **(E)** Bout duration histogram colored by behavioral state; data combined from all animals.

bioRxiv preprint doi: https://doi.org/10.1101/829234; this version posted November 4, 2019. The copyright holder for this preprint (which was not certified by peer review) is the author/funder. All rights reserved. No reuse allowed without permission.

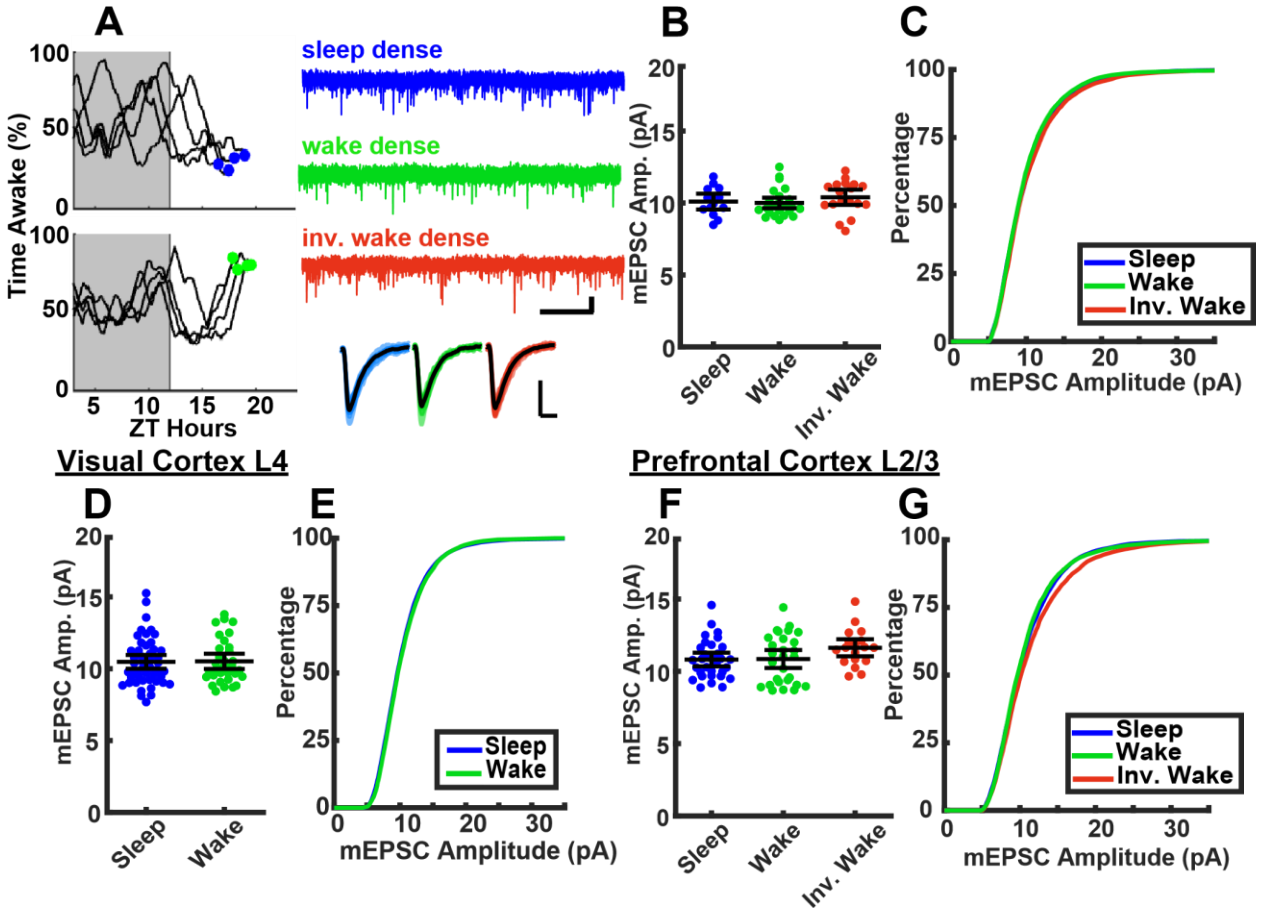

Figure 3. Spontaneous mEPSCs are stable across wake and sleep. (A) Left plots show example behavioral histories as time spent awake of individual animals before slices were taken; dots indicate sleep and wake dense end points. Plots on the right, example mEPSC recording traces; scale bar, 10 pA and 1 second. Cell average mEPSC events; scale bar, 5 pA, 5 ms. **(B)** Data from L2/3 of V1. Left, cell average mEPSC amplitudes; error bars = SEM. Right, cumulative histogram of sampled mEPSC amplitudes. Sleep dense n = 13 cells, 3 animals; wake dense n = 25 cells, 4 animals; inv. wake dense n = 18 cells, 5 animals. **(C)** Data as in (B) but from L4 V1. Sleep dense n = 47 cells, 6 animals; wake dense n = 32 cells, 4 animals. **(D)** Data as in (B) but from L2/3 of PFC. Sleep dense n = 31 cells, 6 animals; wake dense n = 28 cells, 5 animals; inv. wake dense n = 18 cells, 6 animals. PFC Inv. wake to Sleep dense distributions significantly different ($p < 0.05$; KS test).

bioRxiv preprint doi: https://doi.org/10.1101/829234; this version posted November 4, 2019. The copyright holder for this preprint (which was not certified by peer review) is the author/funder. All rights reserved. No reuse allowed without permission.

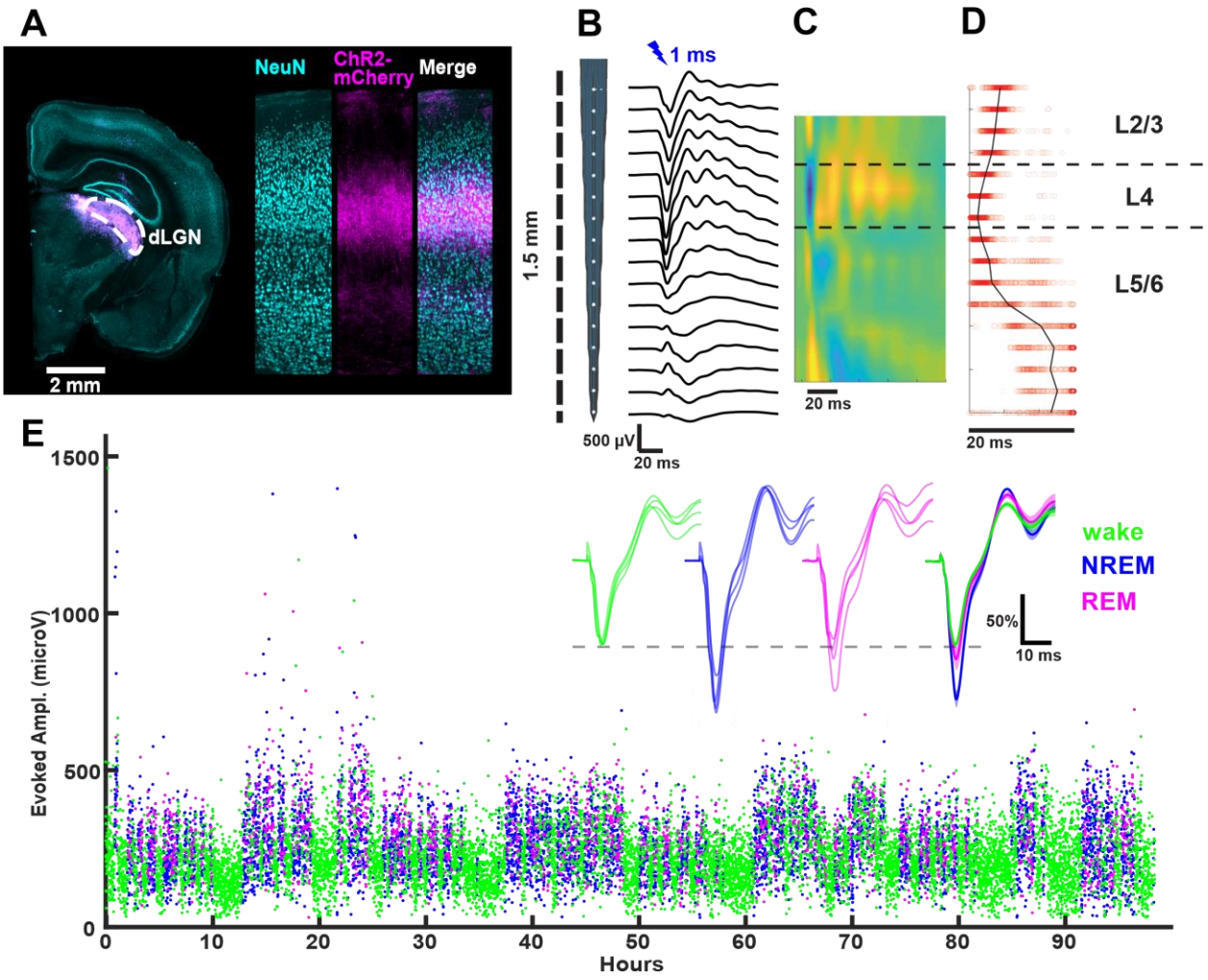

Figure 4. Thalamocortical evoked fEPSPs in V1 . (A) AAV-Chr2-mCherry viral expression targeted to dLGN projects to V1. **(B)** Evoked fEPSPs recorded with a linear silicon array show clear layer-specific waveforms consistently with TC afferent location. **(C)** Current source density heat plot identifies layers; cool colors indicate current sink. **(D)** fEPSP trough latency identifies layers. **(E)** fEPSPs recorded over days in a single freely behaving animal. Amplitude of the response plotted and colored by brain state. Inset, fEPSP waveforms by brain state; individual traces are colored, mean is black. N = 4 animals, recorded for 194 hours.

bioRxiv preprint doi: https://doi.org/10.1101/829234; this version posted November 4, 2019. The copyright holder for this preprint (which was not certified by peer review) is the author/funder. All rights reserved. No reuse allowed without permission.

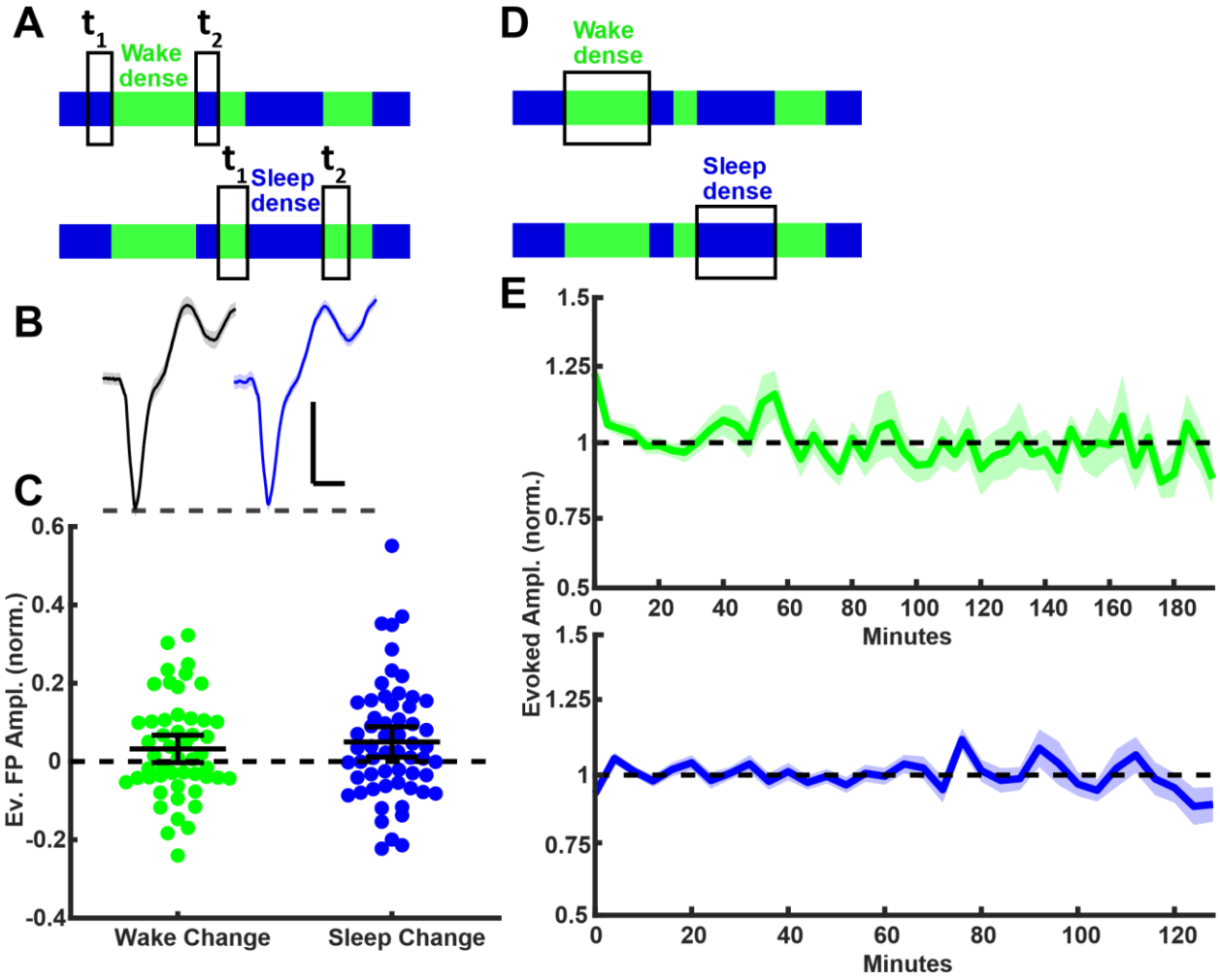

Figure 5. Evoked fEPSPs in freely behaving animals are stable across sleep and wake. **(A)** Schematic showing how fEPSP amplitudes are chosen before and after an extended wake/sleep episode; green indicates wake epochs, blue sleep epochs. **(B)** Example average fEPSP responses before and after a sleep dense episode. **(C)** fEPSP amplitudes are not significantly different before and after sleep or wake episodes. Data from 4 animals recorded for 194 hours total; 58 sleep dense epochs, 50 wake dense epochs. **(D)** Schematic showing tracking of responses during dense episodes. **(E)** fEPSP amplitudes do not show significant changes over the course of sleep/wake episodes. Data from flanked epochs used in (C).

bioRxiv preprint doi: https://doi.org/10.1101/829234; this version posted November 4, 2019. The copyright holder for this preprint (which was not certified by peer review) is the author/funder. All rights reserved. No reuse allowed without permission.

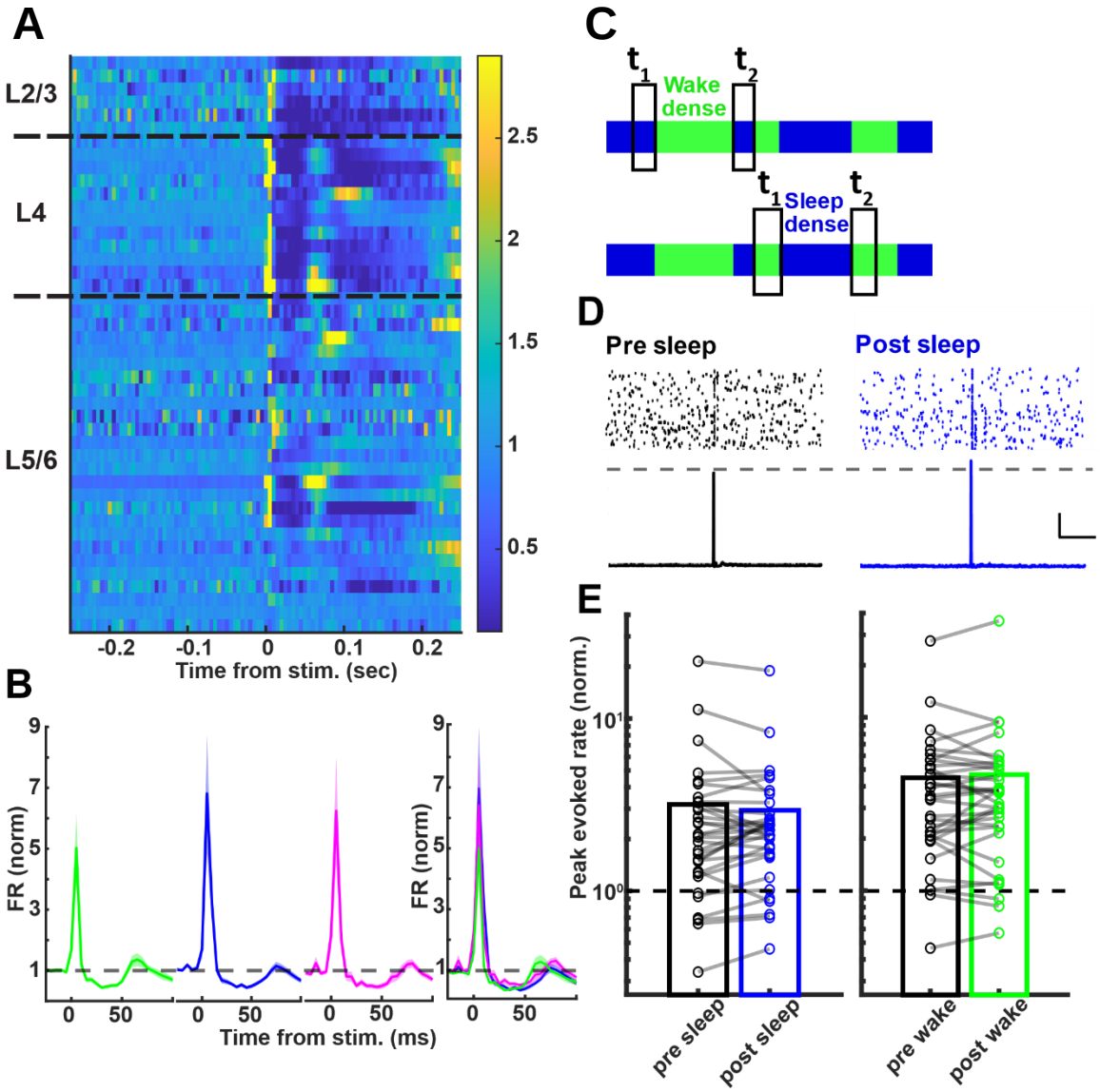

Figure 6. Thalamocortical evoked firing rates are stable across sleep and wake. (A) Evoked spike response to TC stimulation normalized to pre-stimulus baseline; colored by magnitude of response. N = 44 cells (regular spiking units) from 4 animals. **(B)** Evoked spike responses by brain state. Thousands of stimulation responses from 44 cells from 4 animals **(C)** Schematic showing how spike responses before and after sleep/wake dense episodes are chosen. **(D)** Top, example raster plots of a single neuron responding to stimulation before and after sleep. Bottom, average PSTH of same neuron. **(E)** Evoked spike rates show no significant change before and after sleep or wake. N = 44 cells, 4 animals; 58 sleep dense epochs, 50 wake dense epochs.